SP2020_00238

ANALYSIS AND LOW ORDER MODELING OF THE ACOUSTIC DAMPING FOR HIGH-FREQUENCY COMBUSTION INSTABILITIES PREDICTION IN LIQUID ROCKET ENGINES

Alexandre Fougnie[(1),(2)], Thomas Schmitt[(1)], Sébastien Ducruix[(1)]

[(1)] Laboratoire EM2C, CNRS, CentraleSupélec, Université Paris-Saclay, Bâtiment Eiffel, 3 rue Joliot Curie, 91192 Gif-sur-Yvette, France
alexandre.fougnie@centralesupelec.fr
thomas.schmitt@centralesupelec.fr
sebastien.ducruix@centralesupelec.fr

[(2)] CNES, Launchers Directorate, 52 Rue Jacques Hillairet, 75612 Paris Cedex, France

KEYWORDS:

liquid rocket propulsion, thermo-acoustic instabilities, high-frequency instabilities, low order modeling, acoustic damping

ABSTRACT:

The phenomena liable for acoustic damping in thermo-acoustic instabilities in liquid rocket engines are investigated. Modelings to account for the nozzle impedance, in compact hypothesis, and for the visco-thermal losses at walls are derived according to the Galerkin framework, where pressure variations are decomposed over the acoustic eigenmodes. Models are implemented in a low order tool and compared successfully to analytic and numerical predictions. The turbulent/acoustic interaction, responsible for acoustic absorption at the jets, is reviewed, and an in-progress strategy is presented.

1. INTRODUCTION

High frequency combustion instabilities represent one of the main challenging phenomena to predict when designing a new liquid rocket engine, and this since the beginning of the space era [1] [2]. It arises from the coupling between the flames' unsteady heat release, the combustion chamber's acoustics, and the injection dynamics, leading to tremendous pressure oscillations in some configurations. It involves mainly transverse acoustic waves, submitting the flames to transverse oscillating velocity solicitations and the injection units to oscillating mass flow rate. Thus, the prediction of these instabilities is crucial for the safety and nominal running of the engine. However, the global comprehension of the coupling involved still requires substantial analysis of the mechanisms at stake, and consequently the qualification of an engine demands long and expensive real-size tests [3] on dedicated test benches. Progress in numerical simulation permits a more refined physics analysis but can still not faithfully reproduce all the relevant couplings and mechanisms.

Low order methodologies have been actively developed throughout recent years to evaluate the level of instability without requiring massive tests or computations. The numerical cost reduction is achieved by simplifying the physics modeled. In collaboration with CNES and ArianeGroup, EM2C laboratory is developing the StaHF (Stability High Frequency) [4] code based on a modal expansion of the pressure fluctuations over the acoustics eigenmodes [5]. This approach requires models to translate the interactions and behaviors responsible for the evolution of the instabilities. In particular, it is crucial to account for the combustion response to acoustic perturbations and the damping of acoustic waves. From previous work, [1] [4], combustion models have been developed and implemented on low order codes. However, only a little scattered information is available about the acoustic losses within the engine, and no substantial numerical/experimental studies specifically applied to rocket engines with corresponding physical analysis and modeling are available.

Consequently, three mechanisms of acoustic damping are reviewed; nozzle losses, viscous and thermal losses at walls, and turbulence/acoustic interaction. Specific attention about each phenomenon is given in the corresponding section. First, §2 presents some generalities about thermo-

acoustic instabilities. Then, §3 outlines the methodology chosen for the development of the StaHF low order tool. The mechanisms of damping are analyzed and modeled in §4, §5 and §6. Finally, §7 draws a conclusion and some perspective for future work.

2. THERMO-ACOUSTIC INSTABILITIES AND DAMPING GENERALITIES

In the most straightforward linear formulation, the study of the thermo-acoustic stability of a system amounts to the study of the evolution of pressure oscillations p' of pulsation ω in the form of a harmonic oscillator

$$p'(\mathbf{x},t) = p_0(\mathbf{x})e^{-\sigma_p t}\cos(\Omega t), \qquad \text{Eq.1}$$

with $\Omega = \sqrt{\omega^2 - \sigma_p^2}$. The stability is thus linked to the sign of the coefficient σ_p. If $\sigma_p > 0$, p' decreases, and the system is deemed stable, the oscillations are damped. Otherwise, p' increases and the system is unstable. The challenge is to determine the sign of σ_p from the physical phenomena involved. One can decompose the coefficient as [5]

$$\sigma_p = \sum_i \sigma_{\text{phenomena,i}} \qquad \text{Eq.2}$$

with a coefficient of damping, or growth depending on the sign, must be evaluated for each contribution and for a specific acoustic frequency. Classifying the contributions as either producing or destroying acoustic energy, the growth of the instabilities depends on the competition between these two groups, which varies with the acoustic frequencies of interest. In an energetic form, the problem is traditionally written as [6]

$$\frac{\partial E_a}{\partial t} + \int_V \nabla.(p'\mathbf{u}')dV = R_a + D, \qquad \text{Eq.3}$$

with

$$E_a = \int_V \frac{1}{2}\frac{p'^2}{\bar{\rho}\bar{c}} + \frac{1}{2}\bar{\rho}|\mathbf{u}'|^2 dV \qquad \text{Eq.4}$$

the acoustic energy, $\bar{\rho}$ the mean density, $\bar{c}$ the mean sound speed and $\mathbf{u}'$ the acoustic velocity oscillations, $\int_V \nabla.p'\mathbf{u}'dV = \int_S p'\mathbf{u}'.\mathbf{n}dS$ is the acoustic flux at the boundaries,

$$R_a = \int_V \frac{\gamma - 1}{\gamma \bar{p}} p'\dot{q}' dV \qquad \text{Eq.5}$$

the Rayleigh term being the flame response, representative of the coupling between the acoustic perturbation and the combustion, with γ the specific heat ratio, $\bar{p}$ the mean pressure and $\dot{q}'$ the unsteady heat release. D is the dissipated acoustic power. It comes

$$\sigma_p = \frac{D - \int_S p'\mathbf{u}'.\mathbf{n}dS + R_a}{2E_a}. \qquad \text{Eq.6}$$

The previous formulation remains restrictive because the flame does not always act as an excitation source according to its response time [7], and other phenomena can be responsible for the production of acoustic energy.

Another point to mention is the link with acoustic frequencies. The determination of σ and Ω is equivalent to accessing the modifications of the real and imaginary frequencies of the acoustic modes induced by these phenomena, as explained in [5]. The frequency of the m^{th} mode can be decomposed as

$$f_m = f_m^{\mathcal{R}_e} + \delta f_m^{\mathcal{R}_e} + j f_m^{\mathcal{I}_m}, \qquad \text{Eq.7}$$

with $f_m^{\mathcal{R}_e}$ the modal frequency of the normal mode, without source term or boundary conditions (BC), $\delta f_m^{\mathcal{R}_e}$ the deviation from the initial frequency due to combustion, BC, and other phenomena, and $f_m^{\mathcal{I}_m}$ the imaginary part, initially null but rising due to source terms and BC. So

$$\begin{aligned} p'(\mathbf{x},t) &= p_0(\mathbf{x})\mathcal{R}_e\left(e^{-j\omega_m t}\right) \\ &= p_0(\mathbf{x})e^{2\pi f_m^{\mathcal{I}_m} t}\cos(2\pi(f_m^{\mathcal{R}_e} + \delta f_m^{\mathcal{R}_e})t). \end{aligned} \qquad \text{Eq.8}$$

It highlights the link between the imaginary modal frequency and the growth/damping rate, and the modification of the real frequency by the various phenomena present. From a design stage perspective, it is also essential to access the correct values of mode frequencies at which instabilities are likely to occur.

One of the main difficulties in treating instabilities is the numerous phenomena and couplings present within the engine. Also, the transposition of studies on academic experimental benches to real size engines are not straightforwards, frequencies are much higher, the combustion more powerful, and where test benches have from one to a few dozen injectors, real size engines can be teamed to hundreds of injection units. Let us come back to the physical behavior within the engine. Three large families of fluctuation modes evolve in a gas [8], see Fig.1 and interact with each other, mainly in specific areas; the acoustic modes with disturbances propagating at the speed of sound, the vorticity modes, as the vortex from turbulence near the injection, and the entropy modes that are hot spot generated mainly in the flames region. As soon as an average flow is considered, the last two are present, convecting the perturbations. Most studies only consider the evolution of the acoustic modes, but some coupling models exist, such as [9] where the hot spots convected towards the nozzle exit are transformed into acoustic perturbations injected back into the domain. One of the great difficulties of the low order appears to model as well as possible the involved mechanisms, thus including as many as possible relevant couplings that need to be carefully identified while maintaining a clear and numerically-light framework. The main regions responsible for coupling and acoustic generation/destruction are; 1) the flames and injection area, 2) the nozzle with high Mach flow, 3) the walls, and 4) the injection

units. Fig.1 represents in a non-exhaustive and simplified way the main phenomena of interest. However, most of them are out of the scope of the present study. Flame and excitation models have already been developed [1] [4] [10], but few analyses and models concerning the acoustic damping allow an adequate prediction of the level of instabilities. Mainly, the following mechanisms are reviewed [11]

1. the losses at the nozzle region;
2. the visco-thermal losses at walls;
3. the losses from the acoustic/turbulence interaction at the jets location.

Before looking in detail at these different points, the low order framework used to predict the pressure variations is presented, guiding our modeling efforts.

3. LOW ORDER FRAMEWORK

3.1. The low order approach

The low order approach simplifies the conservation equations, applied in general on mesh coarser than for more classical numerical computations as Large Eddy Simulations (LES), in only keeping in the calculation the physical variables and the phenomena of interest regarding the case study. Consequently, the numerical resources needed to perform the analysis are reduced as well as the computation time, allowing to quickly estimate the stability of the configuration of interest for varying geometrical parameters and operative conditions. Without this tool, the LES computations would require disproportionate numerical resources or numerous, long and costly real-size tests on dedicated engines. With a simplified physical representation, the low order approach enables investigating various cases for a reasonable financial and numerical cost.

Several methods have been developed so far for the study of combustion instabilities; as the use of Riemann invariant [12] through acoustic networks, but often limited to longitudinal waves; the Galerkin expansion, by expanding the acoustic perturbations over the acoustic modes [5] recently extended to the state-space approach [13]; the coupled Riemann-Galerkin hybrid approach; or the resolution of the Helmholtz equation using finite elements as in [14].

3.2. Galerkin expansion

The code developed the EM2C laboratory, StaHF [4], is based on the Galerkin expansion, introduced first by [15] and extensively developed by [5]. This method consists in decomposing the acoustic pressure oscillations on the base formed by the acoustic normal eigenmodes of the engine. Temporal and spatial contributions are then isolated. Also it allows to work on complex geometries with longitudinal, transverse and coupled modes. Thus, the pressure oscillations are written as

$$p'(\mathbf{x},t) = \sum_{n=1}^{\infty} \eta_n(t)\Psi_n(\mathbf{x}), \qquad \text{Eq.9}$$

where Ψ_n are the acoustic eigenmodes, and η_n are the temporal evolution of each mode. The particularity of this expansion is to consider the modal base as orthogonal. This condition is met when the modes are computed without source terms and with homogeneous boundary conditions (BC), so that of Neumann where $\nabla\Psi_n(\mathbf{x}_s).\mathbf{n} = 0$ on the boundary, with $\mathbf{x}_s$ located on the boundary, or Dirichlet where $\Psi_n(\mathbf{x}_s) = 0$ on the boundary, or mixed type, with Neumann BC on some parts and Dirichlet BC on others. For simple configurations, the base $(\Psi_n)_{n\geq 1}$ can be determined analytically, but for more complex geometries, the use of a Helmholtz solver is necessary, as AVSP from Cerfacs [14]. As a consequence of the orthogonality, the norm is

$$\int_V \Psi_n\Psi_m dV = \Lambda_n\delta_{nm} \text{ with } \Lambda_n = \int_V \Psi_n^2 dV, \quad \text{Eq.10}$$

which represents the main aspect of the modal expansion. To establish the differential equation that translate the behavior of $(\eta_n)_{n\geq 1}$, and so of p', a first order linearization is applied to the conservation equations of mass Eq.11, momentum Eq.12, energy Eq.13 and the perfect gas equation of state Eq.14 that are

$$\frac{\partial\rho}{\partial t} + \nabla.\rho\mathbf{u} = 0, \qquad \text{Eq.11}$$

$$\rho\left(\frac{\partial\mathbf{u}}{\partial t} + \mathbf{u}.\nabla\mathbf{u}\right) = -\nabla p, \qquad \text{Eq.12}$$

$$\rho T\left(\frac{\partial s}{\partial t} + \mathbf{u}.\nabla s\right) = \dot{q}, \qquad \text{Eq.13}$$

$$p = \rho^\gamma e^{s/c_v}, \qquad \text{Eq.14}$$

with ρ the density, $\mathbf{u} = (u_1, u_2, u_3)$ the velocity vector, p the pressure, T the temperature, s the entropy of the flow, $\dot{q}$ the heat release per unit volume, γ the specific heat ratio and c_v the specific heat of the mixture at constant volume. Each quantity $\mathcal{F}(\mathbf{x},t)$ is decomposed into a mean component $\bar{\mathcal{F}}(\mathbf{x})$ and a fluctuating component $\mathcal{F}'(\mathbf{x},t)$. Then, using a zero Mach hypothesis that state that $\bar{\mathbf{u}}$ is of first order, the pressure differential equation Eq.15 is obtained:

$$\frac{\partial^2 p'(\mathbf{x},t)}{\partial t^2} - \gamma\bar{p}\nabla.(\frac{1}{\bar{\rho}}\nabla p'(\mathbf{x},t)) = (\gamma-1)\frac{\partial\dot{q}'}{\partial t} \quad \text{Eq.15}$$

Then, the expansion Eq.9 is used, with the modes verifying the Helmholtz equation Eq.16 with homogeneous BC, with $\omega_m = 2\pi f_m$ the mode pulsation and f_m its frequency;

$$\gamma\bar{p}\nabla.\left(\frac{1}{\bar{\rho}}\nabla\Psi_m\right) + \omega_m^2\Psi_m = 0. \qquad \text{Eq.16}$$

By considering a finite number of mode N, Eq.15$*\Psi_m$ and Eq.16$*p'$ gives

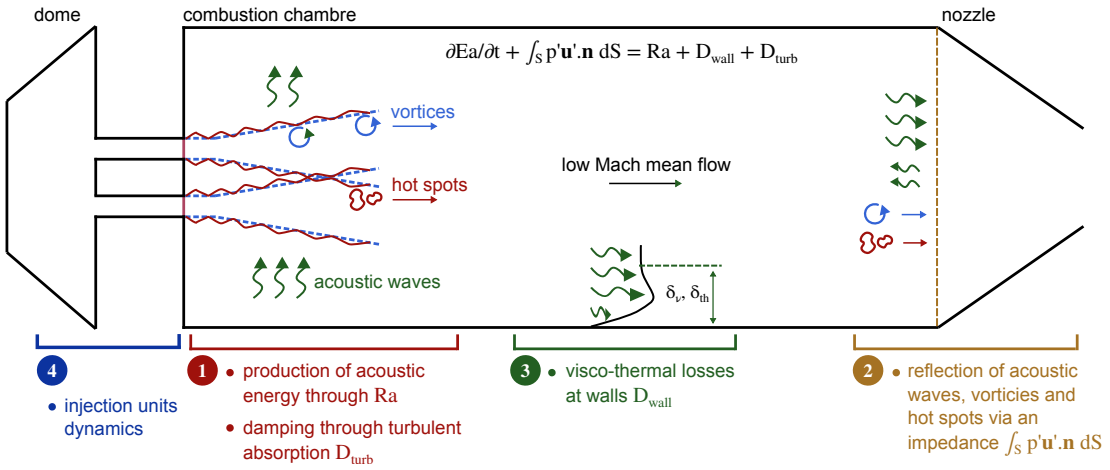

Figure 1: Non-exhaustive schematic representation of some of the mechanisms involved in high frequency combustion instabilities within rocket engines. Mainly, the perturbations source is the flame coupling producing energy via the R_a term. The acoustics is damped at the nozzle location $\nabla.(p'\mathbf{u}')$, near the walls D_{wall} and by interaction with the jets' turbulence D_{turb}.

$$\frac{\partial^2 p'}{\partial t^2}\Psi_m + \omega_m^2 \Psi_m p' + \gamma\bar{p}\nabla.\left(\frac{1}{\bar{\rho}}\nabla\Psi_m\right)p' - \gamma\bar{p}\nabla.\left(\frac{1}{\bar{\rho}}\nabla p'\right)\Psi_m = (\gamma-1)\frac{\partial\dot{q}'}{\partial t}\Psi_m. \quad \text{Eq.17}$$

Then an integration of Eq.17 over the volume V of the domain and the use of the projection Eq.9 give:

$$\sum_{n=1}^{N}\ddot{\eta}_n(t)\int_V \Psi_n\Psi_m dV + \omega_m^2\sum_{n=1}^{N}\eta_n(t)\int_V\Psi_n\Psi_m dV + \int_V \gamma\bar{p}\left(p'\nabla.\left(\frac{1}{\bar{\rho}}\nabla\Psi_m\right) - \Psi_m\nabla.\left(\frac{1}{\bar{\rho}}\nabla p'\right)\right)dV = (\gamma-1)\int_V\frac{\partial\dot{q}'}{\partial t}\Psi_m dV, \quad \text{Eq.18}$$

and using the orthogonality property and the Green identity, Eq.19 is obtained for each mode m;

$$\ddot{\eta}_m(t) + \omega_m^2\eta_m(t) + \frac{1}{\Lambda_m}\int_S \bar{c}^2 p'\nabla\Psi_m.\mathbf{n} - \bar{c}^2\Psi_m\nabla p'.\mathbf{n}dS = \frac{\gamma-1}{\Lambda_m}\int_V\frac{\partial\dot{q}'}{\partial t}\Psi_m dV. \quad \text{Eq.19}$$

At this point, it can be noted that the surface integration term corresponds to the BC and in the energetic formulation Eq.15, to the term $\nabla.(p'\mathbf{u}')$. It will be further discussed and simplified, noted hereafter as S^m_{BC}. Thus,

$$\ddot{\eta}_m(t) + \omega_m^2\eta_m(t) = \frac{\gamma-1}{\Lambda_m}\int_V\frac{\partial\dot{q}'}{\partial t}\Psi_m dV + S^m_{BC}. \quad \text{Eq.20}$$

3.3. Modal amplitude differential equation

On Eq.20, the first term of the right-hand side corresponds to a source term translating the effect of the combustion under an acoustic solicitation. It requires a formulation of $\dot{q}'$, the more common being the sensitive time lag model [1], that supposes the heat release as proportional to the pressure variation, through the interaction index n, but delayed of a time lag τ;

$$\dot{q}'(\mathbf{x},t) = n\frac{\bar{q}}{\bar{u}}u'(\mathbf{x},t-\tau). \quad \text{Eq.21}$$

Other models have been developed later on [4]. More generally, the concept of the Galerkin approach is to develop, as source term, models to account for the combustion, the acoustic damping, some experimental excitation devices, etc, so that Eq.20 writes as

$$\ddot{\eta}_m(t) + \omega_m^2\eta_m(t) = S^m_{comb} + S^m_{damp} + S^m_{exc}. \quad \text{Eq.22}$$

The source terms can be developed based on experimental or numerical considerations through transfer functions for instance. Or, as it will be seen later on, by deriving the present framework including extra terms in the conservation equations, imposing specific conditions for the boundary term in Eq.19 or via energetic considerations (cf §3.4).

3.4. Notes

A few remarks;

1) The mean flow has not been assumed to be zero, but of Mach order 1, so there is no $\bar{\mathbf{u}}$ term explicitly in the presented framework. However, the influence of the mean flow exiting the engine can be accounted through an impedance BC, see §4. The consideration of the high Mach number in the framework is not treated here and will be added later, $M = \bar{u}/\bar{c}$ being of the order of 0.3 in rocket engines.

2) No further discussion will be made on the flame influence and modeling.

3) A parallel can be made with the remarks and formulations of §2. As a general and simplified formulation, the source terms, reduced to a driving and damping component can be written as

$$S^m_{driv} = -2\sigma^m_{driv}\dot{\eta}_m(t) + \Delta\omega^m_{driv}\eta_m(t)$$
$$S^m_{damp} = -2\sigma^m_{damp}\dot{\eta}_m(t) + \Delta\omega^m_{damp}\eta_m(t), \quad \text{Eq.23}$$

so that

$$\ddot{\eta}_m(t) + 2(\sigma^m_{damp} + \sigma^m_{driv})\dot{\eta}_m(t) + (\omega^2_m - \Delta\omega^m_{damp} - \Delta\omega^m_{driv})\eta_m(t) = 0 \quad \text{Eq.24}$$

The phenomenon modeled hereafter can usually be seen as responsible of growth/damping and of frequency shift. In some cases, it is easier to develop a model for the energetic term of Eq.15, then the growth/damping coefficients are found using

$$\sigma^m_{damp} = \frac{D}{2E_a} \text{ and } \sigma^m_{driv} = \frac{R_a}{2E_a}. \quad \text{Eq.25}$$

4. NOZZLE ACOUSTIC LOSSES

This section focuses on applying to our framework an impedance to account for the acoustic losses at the domain boundaries, corresponding to the $\nabla.p'\mathbf{u}'$ term of Eq.15 and S^m_{BC} term of Eq.20. In a rocket engine application, this can be used to model the influence of the nozzle, which is a high Mach region, and therefore where the calculation of modes becomes uncertain because of low Mach hypothesis in Helmholtz solvers.

4.1. Acoustic impedance of the nozzle

The acoustic impedance is defined as

$$\hat{Z}(\mathbf{x}_s, \omega) = \frac{\hat{p}(\mathbf{x}_s)}{\bar{p}\bar{c}\hat{\mathbf{u}}(\mathbf{x}_s).\mathbf{n}}, \quad \text{Eq.26}$$

with the $\mathbf{n}$ the normal vector at the outlet and $\mathbf{x}_s$ the position along the outlet plane. The symbol $\hat{.}$ denotes a complex quantity. The impedance is linked to a reflection coefficient $\hat{R}$, ratio between the reflected acoustic pressure amplitude and the incident acoustic wave as

$$\hat{R} = \frac{\hat{Z} - 1}{\hat{Z} + 1}. \quad \text{Eq.27}$$

Compact nozzle For a compact nozzle, meaning the acoustic wavelengths are large compared to the nozzle dimensions, the impedance is a real number and independent of the acoustic frequency. Z is a function of the Mach number M_1 at the nozzle inlet, proposed by [9], for a supersonic nozzle ($M_t = 1$ at the throat). The reflection coefficient is

$$R_{sup} = \frac{1 - \frac{1}{2}(\gamma - 1)M_1}{1 + \frac{1}{2}(\gamma - 1)M_1}, \quad \text{Eq.28}$$

giving,

$$Z = \frac{2}{(\gamma - 1)M_1}. \quad \text{Eq.29}$$

For a subsonic nozzle, where the flow does not become supersonic,

$$R_{sub} = \frac{M_2 - M_1}{1 - M_1}\frac{1 + M_1}{M_1 + M_2}\frac{1 - \frac{1}{2}(\gamma - 1)M_1M_2}{1 + \frac{1}{2}(\gamma - 1)M_1M_2}, \quad \text{Eq.30}$$

with M_2 the Mach number at the nozzle outlet. Fig.2 shows the dependance of Z with M_1, for both subsonic and supersonic nozzles. For low Mach numbers $M_1 < 0.3$, the impedance is large $Z > 20$ ($\gamma = 1.4$) for the supersonic configuration and small $Z < 0.1$ for the subsonic one. Thus, in the compact hypothesis, for a chocked nozzle (supersonic), the nozzle behave acoustically as a solid wall, validating the mode computation using a Neumann BC $\mathbf{u}'(\mathbf{x}_s).\mathbf{n}$. On the contrary, a subsonic nozzle would require to compute the normal modes using a Dirichlet condition $p'(\mathbf{x}_s) = 0$.

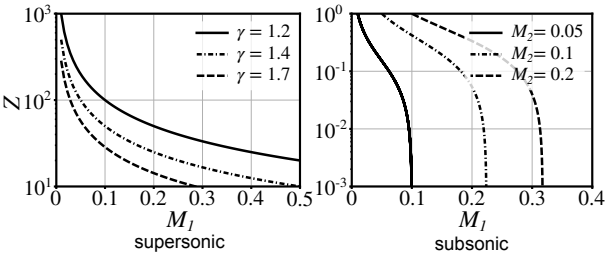

Figure 2: Representative impedance of a supersonic (left) and subsonic (right) nozzle, with respect to the inlet Mach number, from [9]

Non-compact nozzle The case of a non-compact nozzle is more complex to treat because it is necessary to account for the geometry of the nozzle and that the impedance becomes a complex value and depend on the acoustic frequency. First, [16] developed a 3D admittance nozzle theory for constant longitudinal amplitude oscillations, extended by [17] to account for amplitude variations. Then, [9] proposed an acoustic and entropic impedance using a linearly varying velocity in the nozzle. Later, [18] and [19] conceived a robust numerical methodology based on the Magnus expansion, then extended by [20] to be applied to transverse waves. Fig.3 shows the real and imaginary part of the nozzle reflection coefficient with respect to the acoustic frequency for longitudinal perturbations, for an arbitrary combustor with nozzle geometry. Similar profiles are found in the given references. It shows that R evolves from a high value $\mathcal{R}_e(R) \approx 1$, corresponding to the value found using the compact nozzle hypothesis, to values close to $\mathcal{R}_e(R) \approx 0$. Also $\mathcal{I}_m(R)$ undergoes important evolution. In other references, for specific nozzle geometry and velocity profile, the reflection coefficient becomes negative in some frequency ranges. Thus the nozzle acts acoustically closer to a chocked nozzle (as $\mathbf{u}'(\mathbf{x}_s).\mathbf{n} = 0$) for certain frequencies and for other frequencies, closer to an open exit $p'(\mathbf{x}_s) = 0$. The longitudinal waves are highly damped and the BC influences the modes' shape.

It underlines one of the main limitations of

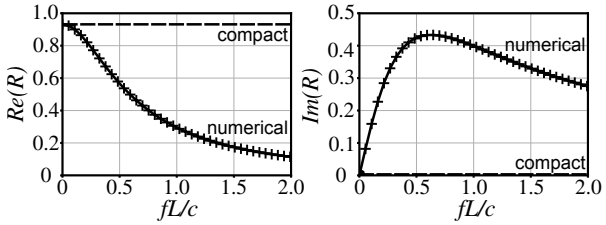

Figure 3: Real (left) and imaginary (right) part of the reflection coefficient, compute with the NOZZLE tool [18] of AVSP, for an arbitrary nozzle geometry with a chocked nozzle. f is the frequency, L the nozzle length and c the sound speed.

the Galerkin approach; limited to modes where $\mathbf{u}'(\mathbf{x}_s).\mathbf{n} = 0$ or $p'(\mathbf{x}_s) = 0$ conditions have been imposed at the exit when computing the mode to ensure the orthogonality property. However, the impedance BC would require modes computed using both conditions for some applications, depending on the frequency. A solution has been recently proposed to overcome this issue using a state-space approach and a dual base decomposition [13].

In the case of a rocket engine, it has been shown that the nozzle losses are high and preponderant for the longitudinal modes, but of secondary importance for transverse and coupled modes [21], which are the principal modes of interest in high-frequency instabilities, and that the compact nozzle model of [9] can be applied to transverse modes [22]. The damping is then to be dominated by the phenomena near the plate injection as the turbulence/acoustic interaction (see §6). The hypothesis of a compact nozzle is thus retained and the influence of the modal shape modification is neglected for the proposed modeling.

4.2. Low order Z model

The hereafter model is restricted to $\hat{Z}$ as a real number, following the compact hypothesis, but is also valid for a complex impedance, not shown here for clarity. The modeling is based on the approach suggested in [5] [23] [24].

$|\mathbf{Z}| > 1$ For $|Z| > 1$, the modal shape is close to the shape computed using a $\nabla\Psi_m.\mathbf{n} = 0$ condition on the boundary of interest. The base used in the low order framework is thus verifying $\nabla\Psi_m.\mathbf{n}(\mathbf{x}_s) = 0$ and the modes are still orthogonal. To account for the impedance, the condition $\nabla p'.\mathbf{n} = -f(Z)$ has to be imposed as BC. The corresponding term of Eq.20 is, supposing $\bar{c}$ uniform on the boundary surface,

$$S^m_{BC} = -\frac{\bar{c}^2}{\Lambda_m}\int_S f(Z)\Psi_m dS. \qquad \text{Eq.31}$$

The relation

$$\nabla p'.\mathbf{n} = -j\omega\bar{\rho}\mathbf{u}'.\mathbf{n} \qquad \text{Eq.32}$$

is obtained from Eq.12, giving with the impedance formulation,

$$f(Z) = \frac{j\omega}{\bar{c}Z}p'. \qquad \text{Eq.33}$$

Thus the source term becomes

$$\begin{aligned} S^m_{BC} &= -\frac{\bar{c}}{\Lambda_m Z}\int_S j\omega p'\Psi_m dS \\ &= -\frac{\bar{c}}{\Lambda_m Z}\sum_{n=1}^{N}\dot{\eta}_n\int_S \Psi_n\Psi_m dS. \end{aligned} \qquad \text{Eq.34}$$

$|\mathbf{Z}| < 1$ For $|Z| < 1$, the modal shape is close to the shape computed using a $\Psi_m = 0$ BC. However p' is not assumed null on the boundary and the new relation $p'(\mathbf{x}_s) = -g(Z)$ is imposed. Similarly, the source term is

$$S^m_{BC} = \frac{\bar{c}^2}{\Lambda_m}\int_S g(Z)\nabla\Psi_m.\mathbf{n}dS, \qquad \text{Eq.35}$$

and the g relation is now

$$g(Z) = \frac{\bar{c}Z}{j\omega}\nabla p'.\mathbf{n}. \qquad \text{Eq.36}$$

Consequently, it comes, using $\int_t \eta_n dt = -\frac{1}{\omega_n^2}\dot{\eta}_n$,

$$\begin{aligned} S^m_{BC} &= -\frac{\bar{c}^3 Z}{\Lambda_m}\int_S \frac{1}{j\omega}\nabla p'.\mathbf{n}\nabla\Psi_m.\mathbf{n}dS \\ &= \frac{\bar{c}^3 Z}{\Lambda_m}\sum_{n=1}^{N}\frac{\dot{\eta}_n}{\omega_n^2}\int_S \nabla\Psi_n.\mathbf{n}\nabla\Psi_m.\mathbf{n}dS. \end{aligned} \qquad \text{Eq.37}$$

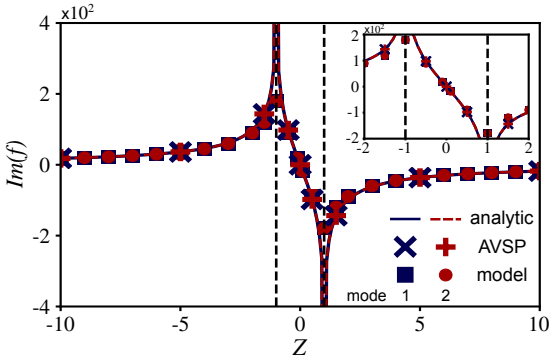

Figure 4: Comparison of the predicted imaginary frequency on a 1D domain, for a real impedance imposed on one side, from analytic, numerical and model.

1D verification The previously obtained model is applied to the one dimensional geometry of [14], of length $L = 0.4\text{m}$ and $\bar{c} = 450\text{m}\,\text{s}^{-1}$, where the impedance is applied on one side of the domain. The imaginary frequencies predicted by the analytic analysis, the AVSP solver [14] and the low order model are compared Fig.4. The imaginary frequencies arise from the impedance, well represented by the model Eq.34 for instance, reduce to a 1 mode equation

$$\ddot{\eta}_m + \underbrace{\frac{\bar{c}}{\Lambda_m Z}\int_S \Psi_m^2 dS}_{2\sigma_{BC}^m = -4\pi f_m^{\mathcal{I}_m}} \dot{\eta}_m + \omega_m^2 \eta_m = 0. \qquad \text{Eq.38}$$

For positive $Z > 0$, $f_m^{\mathcal{I}_m}$ is negative corresponding to a positive σ_{BC}^m, meaning acoustic energy exits through the nozzle, pressure oscillations are damped. Also, $f_m^{\mathcal{I}_m}$ is independent of the mode number and the model indicates that Z real does not produce a frequency shift, other than the one present in the pseudo-pulsation, results in agreements with [14]. However, the model lacks of prediction near the value $|Z| = 1$ for the interval $2 > |Z| > 0.5$. But this interval is satisfactory for transverse acoustic wave in liquid rocket engines [21].

3D comparison The modeled source term is applied on a cylindrical geometry, representative of a rocket engine, and corresponding to the BKD test bench dimensions [25], for a sound speed of $\bar{c} = 1300\,\mathrm{m\,s^{-1}}$. The nozzle is truncated because it is a high Mach region, and a real positive impedance is applied at the location of the nozzle entrance. Imaginary frequencies are computed with the solver AVSP applying the impedance BC and converted into a damping coefficient σ_{BC}^m for the first longitudinal 1L and transverse 1T modes. Then, the 1L and 1T modes have been computed using a homogeneous Neumann BC for the nozzle (for the case $|Z| > 1$ is applied, designated as Neumann-like mode) and for a homogeneous Dirichlet BC for the nozzle (for the case $|Z| < 1$ is applied, designated as Dirichlet-like mode). The low order impedance model implemented in StaHF is applied for a wide range of Z values and the resulting damping is compared to the numerical (AVSP) solution Fig.5. The values of impedance presented here do not correspond to a specific engine loading point, but were set to cover a wide range of values. There is a satisfactory agreements between the low order predictions and the Helmholtz solver results.

Modal coupling at the boundary The present model benefits from the summation over each modal amplitudes seeing in Eq.34 and Eq.37. It signifies that the impedance influence over a specific mode is dependent on the temporal evolution of the other modes, and the damping coefficient σ_{BC}^m is time-dependent, having a more sophisticated form than in Eq.38. According to this formulation, there is a modal coupling at the boundary. Such modeling allows reproducing physical wave behavior, such as the propagation of a traveling wave in an impedance tube, with reflection on one of the tube sides, having a given impedance value. This example is not represented here to remain succinct, but without this modal coupling, the reflection would not happen, and the wave would be constantly damped through the propagation within the tube since σ_{BC}^m is constant for each mode (as in Eq.38). The modal coupling also explains that the BC can be a source of modal non-orthogonality because of interdependence [14].

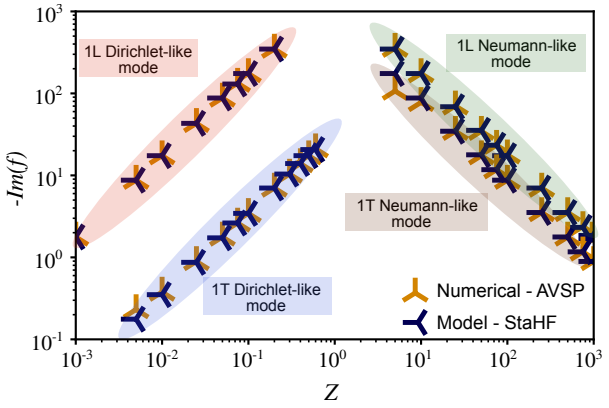

Figure 5: Comparison of the imaginary frequency predicted from numerical analysis (AVSP) and from the StaHF model, for both 1L and 1T modes in a cylindrical geometry at dimension close to the BKD test bench, where a real impedance is imposed at the exit.

5. VISCOUS AND THERMAL DISSIPATION AT WALLS

5.1. Generalities

The viscous losses arise from a no-slip condition at the wall interface. The acoustic velocity takes a certain profile in the acoustic viscous boundary layer δ_ν expressed as

$$u'(x,z,t) = u_x(x)\left[e^{-\frac{y}{\delta_\nu}}\cos\left(\omega t - \frac{y}{\delta_\nu}\right) - \cos(\omega t)\right], \qquad \text{Eq.39}$$

with

$$\delta_\nu = \sqrt{\frac{2\nu}{\omega}}, \qquad \text{Eq.40}$$

ν being the kinematic viscosity, according to the formalism shown in Fig.6. The velocity gradient between the bulk region and the wall leads to a shear stress, and consequently dissipation by friction. Thermal losses are due to the isothermal wall condition, with acoustic oscillations considered as adiabatic[1]. This adiabatic condition is verified when λ_a, the acoustic wavelength, satisfies $\lambda_a > 2\pi D_{th}/c$, which is always true in a rocket engine, where D_{th} is the thermal diffusivity. As for the acoustic velocity, there is a temperature gradient between the wall surface and the acoustic temperature oscillations outside the boundary layer. Thus an oscillating heat flux appears, leading to thermal losses. The acoustic thermal boundary layer δ_{th} is defined as

[1] Adiabatic acoustic is the classical characteristic of the acoustics. It means that the rate of acoustic change in the medium is fast enough so that no heat exchange happens between within the medium. For very high frequencies, the acoustic oscillations are no longer adiabatic but isothermal.

$$\delta_{th} = \sqrt{\frac{2D_{th}}{\omega}}. \qquad \text{Eq.41}$$

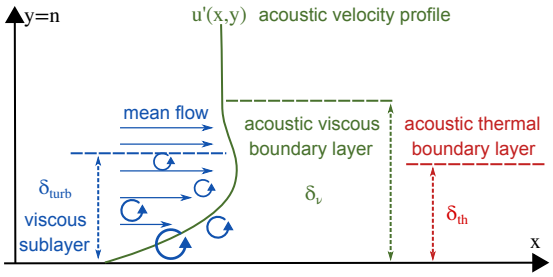

Figure 6: Representation of the acoustic viscous and thermal boundary layers, with the near-wall velocity profile, along the viscous sublayer.

[26] first predicted the sound attenuation in a tube of standing wave without mean flow with a simple formulation. A wider modeling, applicable for any geometries has been proposed by [27] based on the formalism of Eq.6. The viscous σ_ν and thermal σ_{th} damping coefficients are expressed as

$$\sigma_\nu = \frac{\int_S \left\langle \frac{de}{dt} \right\rangle_\nu dS}{2E_a} \text{ and } \sigma_{th} = \frac{\int_S \left\langle \frac{de}{dt} \right\rangle_{th} dS}{2E_a}, \qquad \text{Eq.42}$$

V being the volume of the domain and S the surface of hard walls. The energy derivatives are

$$\left\langle \frac{de}{dt} \right\rangle_\nu = \frac{1}{2}\bar{\rho}u_x^2\sqrt{\frac{\omega\nu}{2}} \qquad \text{Eq.43}$$

and

$$\left\langle \frac{de}{dt} \right\rangle_{th} = \frac{1}{2}(\gamma-1)\frac{p'^2}{\bar{\rho}\bar{c}^2}\sqrt{\frac{\omega D_{th}}{2}}. \qquad \text{Eq.44}$$

This formulation is adaptable for any geometry and can be implemented in low order codes, but it does not account for the effect of the mean flow and turbulence near the walls. [28] extended the losses formulation to the dissipation over an infinite plane, considering the impact of the wall turbulent shear flow for low Mach number. The complete formulation is not presented here, but the result of the influence of the near-wall turbulence in represented Fig.7. Π is the damping per area unit taking into account the turbulence, Π_0 is the no-flow approximation, and v_+ is the friction velocity. It can be seen that for large values of $\omega\nu/v_+^2$, meaning when the turbulence is weak and/or the acoustic frequency is large enough, the influence of the turbulence on the sound dissipation is negligible. It corresponds to a configuration wherein Fig.6 the viscous sublayer is large compared to the acoustic boundary layer $\delta_{turb} \gg \delta_\nu$. However, for high turbulent configurations, when the boundary layers are similar to $\delta_{turb} \approx \delta_\nu$, omitting the turbulent shear flow impact can lead to underestimation of the damping of several factors.

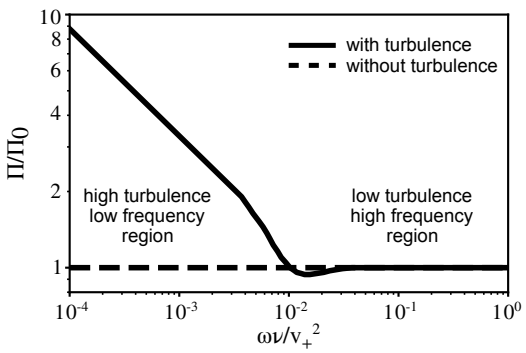

Figure 7: damping rate per surface area with the influence of wall turbulence Π scaled by the damping rate without considering turbulence Π_0, with respect to $\omega\nu/v_+^2$ measuring the acoustic/turbulence intensity, from [28].

5.2. Low order formulation

A derivation of a model for viscous and thermal effects is proposed, using the Galerkin expansion. First, the viscous stress tensor $\underline{\underline{\tau}}$ is added on the conservation equation Eq.12, and the derivation of the acoustic equation, with the modal projection gives

$$\ddot{\eta}_m + \omega_m^2\eta_m - \frac{1}{\Lambda_m}\int_S \bar{c}^2\Psi_m \boldsymbol{\nabla} p'.\mathbf{n}dS = \\ -\frac{1}{\Lambda_m}\int_V \gamma\bar{p}\nabla.\left(\frac{1}{\bar{\rho}}\nabla.\underline{\underline{\tau}}'\right)\Psi_m dV. \qquad \text{Eq.45}$$

The boundary term is simplified using $\nabla\Psi_m.\mathbf{n} = 0$ but the second part of the term is kept to apply the viscous BC condition at the wall $\boldsymbol{\nabla} p'.\mathbf{n} = (\nabla.\underline{\underline{\tau}}').\mathbf{n}$. After some calculations and expressing the tangential acoustic velocity at the wall, similarly as [5], it comes

$$\ddot{\eta}_m + \omega_m^2\eta_m = \underbrace{-\frac{\bar{c}^2}{\Lambda_m}\sqrt{\frac{\omega_m\nu}{2}}\frac{1}{\omega_m^2}\int_S (\nabla^t\Psi_m)^2 dS}_{\text{damping term } 2\sigma_\nu^m}\dot{\eta}_m, \qquad \text{Eq.46}$$

where $\nabla^t\Psi_m$ it the tangential gradient of the m mode at the wall. Similarly, by keeping the thermal term $\nabla.\mathbf{q}_f = -\nabla.(\lambda\boldsymbol{\nabla}T')$ in Eq.12, it comes

$$\ddot{\eta}_m + \omega_m^2\eta_m = -\frac{1}{\Lambda_m}\int_V (\gamma-1)\frac{\partial\nabla.\mathbf{q}_f}{\partial t}\Psi_m dV. \qquad \text{Eq.47}$$

Then using properties on the acoustic temperature gradient explained in [29], the source term due to thermal losses at wall writes

$$\ddot{\eta}_m + \omega_m^2\eta_m = \underbrace{-\frac{1}{\Lambda_m}(\gamma-1)\sqrt{\frac{D_{th}\omega_m}{2}}\int_S \Psi_m^2 dS}_{\text{damping term } 2\sigma_{th}^m}\dot{\eta}_m \qquad \text{Eq.48}$$

Application The models Eq.46 and Eq.48 are applied analytically and numerically on tube and box

geometries, and compared to prediction of [27]. The comparison shows satisfactory results with relative errors of less than $10^{-2}\%$ for the computed damping rate. In particular, for all the presented modeling (StaHF, [26] and [27]), the damping coefficient writes, for a tube of radius R and length L

$$\sigma_m = \frac{1}{R}\sqrt{\frac{\omega_m \nu}{2}} + \frac{(\gamma-1)}{R}\sqrt{\frac{\omega_m D_{th}}{2}}\left(1+\frac{2R}{L}\right). \quad \text{Eq.49}$$

6. WORK IN PROGRESS: TURBULENCE/ACOUSTIC INTERACTION

The last presented phenomenon identified as responsible for the damping of acoustic waves, except the coupling with the combustion, is the interaction between the transverse acoustic perturbations and the turbulence near the injection plate, due to the jets. When the turbulence flow at the injection units' outlet is submitted to transverse acoustic velocity fluctuations, part of the acoustic energy is absorbed and redirected to turbulent energy [30]. Depending on the characteristics of the turbulence and acoustics, sound waves impose stretching to vorticies, transferring energy [31]. Besides absorption, scattering and refraction of the incoming waves take place. Part of the incident wave is redistributed towards other acoustic frequencies and directions of propagation [32] [33], as represented in Fig.8. The scattering and reflection phenomena participate in the modal coupling between the longitudinal and transverse acoustics modes, following §2, but are not of concern in the present study.

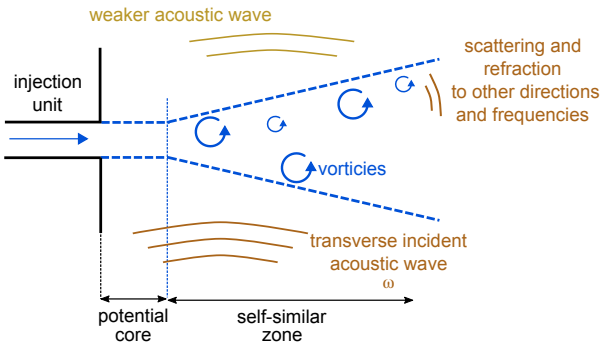

Figure 8: Transverse acoustic wave through a turbulent jet; some of the acoustics is absorbed by the turbulence or scattered to other directions of propagation and frequencies.

Most studies do not consider the combustion process in the study of this interaction. It simplifies the analysis to characterize the acoustic environment of the system by accounting for the turbulent flow. The combustion has to be added a-posteriori after mastering the turbulence/acoustic interaction in a cold-flow environment. Moreover, the referred literature focuses mainly on the absorption of sound generated from the turbulence to evaluate the noise emitted within internal engines.

6.1. Term responsible for absorption

Following the approach of [30], a specific procedure is applied to the conservation equations of Navier-Stokes. First, each quantity is decomposed into a mean, an acoustic and a turbulent contribution, as suggested in [8]. The signal $\mathcal{F}(\mathbf{x},t)$ is expressed as

$$\mathcal{F}(\mathbf{x},t) = \bar{\mathcal{F}}(\mathbf{x}) + \mathcal{F}'(\mathbf{x},t) + \tilde{\mathcal{F}}(\mathbf{x},t), \quad \text{Eq.50}$$

$\bar{\mathcal{F}}(\mathbf{x})$ being the mean component, $\mathcal{F}'(\mathbf{x},t)$ the turbulent component and $\tilde{\mathcal{F}}(\mathbf{x},t)$ the acoustic component. The time average operator $\bar{.}$ defines the mean component and the phase average $\langle . \rangle$ the acoustic one,

$$\overline{\mathcal{F}'} = \bar{\tilde{\mathcal{F}}} = 0 \text{ and } \langle \mathcal{F} \rangle = \bar{\mathcal{F}} + \tilde{\mathcal{F}}. \quad \text{Eq.51}$$

The velocity field is decomposed into the three contributions; $\mathbf{u} = \bar{\mathbf{u}} + \mathbf{u}' + \tilde{\mathbf{u}}$. The mean and turbulent velocity fields are supposed divergence free, $\partial \bar{u}_i/\partial x_i = \partial u_i'/\partial x_i = 0$ (with a summation index notation), and the acoustic fields irrotational, $\nabla \times \tilde{\mathbf{u}} = 0$. The pressure and density fluctuations are supposed to be mainly from acoustic origin, thus $p = \bar{p} + \tilde{p}$, and $\rho = \bar{\rho} + \tilde{\rho}$, using the approximation $\bar{\rho}(1+\tilde{\rho}/\bar{\rho}) \approx \bar{\rho}$. The momentum conservation Eq.12 writes, keeping the viscous stress term,

$$\frac{\partial u_i}{\partial t} + u_j \frac{\partial u_i}{\partial x_j} + \frac{1}{\rho}\frac{\partial p}{\partial x_i} = \frac{1}{\rho}\frac{\partial \tau_{ij}}{\partial x_j}, \quad \text{Eq.52}$$

and applying time and phase average operators, the equation for the temporal evolution of u_i' and $\tilde{u}_i$ are isolated, giving

$$\begin{aligned}\frac{\partial u_i'}{\partial t} =& -\bar{u}_j \frac{\partial u_i'}{\partial x_j} - u_j' \frac{\partial \bar{u}_i}{\partial x_j} - u_j' \frac{\partial \tilde{u}_i}{\partial x_j} - \tilde{u}_j \frac{\partial u_i'}{\partial x_j} \\ &+ \frac{\partial}{\partial x_j}\left(\langle u_i' u_j' \rangle - u_i' u_j'\right) + \frac{1}{\bar{\rho}}\frac{\partial \tau_{ij}'}{\partial x_j}\end{aligned} \quad \text{Eq.53}$$

and

$$\begin{aligned}\frac{\partial \tilde{u}_i}{\partial t} =& -\bar{u}_j \frac{\partial \tilde{u}_i}{\partial x_j} - \tilde{u}_j \frac{\partial \bar{u}_i}{\partial x_j} - \frac{\partial}{\partial x_j}\left(\langle u_i' u_j' \rangle - \overline{u_i' u_j'}\right) \\ &+ \frac{\partial}{\partial x_j}\left(\overline{\tilde{u}_i \tilde{u}_j} - \tilde{u}_i \tilde{u}_j\right) - \tilde{u}_i \overline{\frac{\partial \tilde{u}_j}{\partial x_j}} + \tilde{u}_i \frac{\partial \tilde{u}_j}{\partial x_j} \\ &- \frac{1}{\bar{\rho}}\frac{\partial \tilde{p}}{\partial x_i} + \frac{1}{\bar{\rho}}\frac{\partial \tilde{\tau}_{ij}}{\partial x_j},\end{aligned} \quad \text{Eq.54}$$

Then, by multiplying Eq.53 by u_i', and Eq.54 by $\tilde{u}_i$, phase averaging and time averaging, it comes the conservation equations for the kinetic energy $\overline{u_i' u_i'}$ and for the velocity part of the acoustic energy $\overline{\tilde{u}_i \tilde{u}_i}$;

$$\begin{aligned}\frac{1}{2}\frac{\partial \overline{u_i' u_i'}}{\partial t} =& -\frac{1}{2}\bar{u}_j \frac{\partial \overline{u_i' u_i'}}{\partial x_j} - \overline{u_i' u_j'}\frac{\partial \bar{u}_i}{\partial x_j} - \frac{1}{2}\frac{\partial \overline{u_i' u_i' u_j'}}{\partial x_j} \\ &- \underbrace{\overline{\langle u_i' u_j' \rangle \frac{\partial \tilde{u}_i}{\partial x_j}}}_{\text{term of interest}} - \frac{1}{2}\overline{\tilde{u}_j \frac{\partial \langle u_i' u_i' \rangle}{\partial x_j}} + \overline{\frac{u_i'}{\bar{\rho}}\frac{\partial \tau_{ij}'}{\partial x_j}}\end{aligned} \quad \text{Eq.55}$$

and

$$\frac{1}{2}\frac{\partial\overline{\tilde{u}_i\tilde{u}_i}}{\partial t} = -\frac{1}{2}\bar{u}_j\frac{\partial\overline{\tilde{u}_i\tilde{u}_i}}{\partial x_j} - \overline{\tilde{u}_i\tilde{u}_j}\frac{\partial\bar{u}_i}{\partial x_j} + \frac{1}{2}\overline{\tilde{u}_i\tilde{u}_i\frac{\partial\tilde{u}_j}{\partial x_j}} - \frac{\partial\overline{\tilde{u}_i\langle u_i'u_j'\rangle}}{\partial x_j} + \underbrace{\overline{\langle u_i'u_j'\rangle\frac{\partial\tilde{u}_i}{\partial x_j}}}_{\text{term of interest}} - \frac{1}{2}\frac{\partial\overline{\tilde{u}_i\tilde{u}_i\tilde{u}_j}}{\partial x_j} - \overline{\frac{\tilde{u}_i}{\bar{\rho}}\frac{\partial\tilde{p}}{\partial x_i}} + \overline{\frac{\tilde{u}_i}{\bar{\rho}}\frac{\partial\tilde{\tau}_{ij}}{\partial x_j}} \qquad \text{Eq.56}$$

The term $\overline{\langle u_i'u_j'\rangle\partial\tilde{u}_i/\partial x_j}$ is identified as "term of interest" in both Eq.55 and Eq.56. It is the only similar term in both equations, with a $-$ sign for the turbulent energy evolution and a $+$ sign for the acoustic energy, meaning it represents a transfer of energy from the acoustic to the turbulence (or the other way depending on the sign), due to the acoustic/turbulence interaction. Consequently, studies have proposed formulations for this term, either for a general application [33] or especially to predict the enhancement of the acoustic absorption near the walls [28] [34] retrieving the results of Fig.7.

6.2. Model from literature

Some analyses have derived an analytic estimate of the absorption of the sound generated aerodynamically by a jet. At an arbitrary point in the jet, the sound is emitted due to vortices, and propagates through the jet's turbulence, which absorbs part of it. The objective was to provide the Lighthill theory, which predicts the generation of noise by turbulence, with the contribution of absorption. Considering isotropic homogeneous turbulence, [35] used the viscoelastic property of the turbulence. Under the effect of an acoustic disturbance, the turbulence is stretched and then relaxes to return to isotropy. Energy is given to the turbulence during strain and dissipated by viscous effect. Thus, the viscoelastic property implies that the turbulence, and thus the Reynolds stress, has a memory of its past state through a relaxation time. Based on the local increase in sound velocity due to deformation of the turbulence, [35] predicted a formulation for the damping coefficient;

$$\sigma_{\text{turb}} \simeq \frac{\omega}{5}\frac{M_{\text{rms}}^2 f_t}{1+f_t^2}, \qquad \text{Eq.57}$$

with ω the acoustic pulsation, f_t a reduced frequency such that $f_t = \Omega_t/\omega$, with Ω_t related to the return to isotropy time, and $M_{\text{rms}} = \overline{u_i^2}/\bar{c}$ the root mean square (RMS) Mach number. Considering also a viscoelastic turbulence and manipulating Eq.55 to evaluate the term $\overline{\langle u_i'u_j'\rangle\partial\tilde{u}_i/\partial x_j}$, [33] obtained the following estimation;

$$\sigma_{\text{turb}} \simeq 2.3\frac{\epsilon}{\bar{c}^2}, \qquad \text{Eq.58}$$

equivalent to Eq.57 at high frequencies ($\omega \gg \Omega_t$), using the hypothesis that $\Omega_t \sim \epsilon/\overline{u_i^2}$, and ϵ being the turbulent dissipation rate. With a different approach, [31] used the Lighthill equation, splitting the velocity field into an initial turbulent component and a total contribution caused by the wave. The estimation made leads to, at high frequency and as suggested by previous studies,

$$\sigma_{\text{turb}} \sim \frac{\epsilon}{\bar{c}^2}. \qquad \text{Eq.59}$$

In this case, the absorption will not depend on the acoustic frequency but the characteristics of the turbulence. An estimation at low frequency is also made, but it is necessary to determine what low and high frequency mean regarding the combustion instability application. Also, the objective is to estimate this absorption coefficient for an imposed acoustic solicitation, both in frequency and amplitude. Therefore, an approach is needed to vary the acoustics as a function of the resonant modes (in connection with the Galerkin method), change the turbulence as a function of the jet's position, and test the hypothesis of isotropic homogeneous turbulence.

6.3. Ongoing study

The turbulence component of the velocity is generated using a spectral method of [36] for homogeneous isotropic turbulence, and the non-isotropic character within the jet can be achieved using the method of [37]. The generation procedure demands knowing the specificity of the turbulence, including turbulent kinetic energy k, dissipation rate ϵ, and the ($\overline{u'^2}$ compared to $\overline{v'^2}$ and $\overline{w'^2}$) RMS values for the anisotropy. The present work focuses on the quality of the turbulent velocity field generation and the phase averaging of the velocity signal analytically.

6.4. Remarks

The same process of averaging can be applied to obtain the mean flow evolution, as in §6.1. Without further details, the term $\overline{\tilde{u}_i\tilde{u}_j}\frac{\partial\bar{u}_i}{\partial x_j}$ appears as a source term in the mean flow equation, and is also in Eq.56, with the opposite sign, translating an exchange of energy between the non-uniform mean flow and the acoustics. An equivalent term is found to link the mean flow with the turbulent level; $\overline{u_i'u_j'}\frac{\partial\bar{u}_i}{\partial x_j}$ corresponding to the production of vorticity.

7. SUMMARY AND CONCLUSION

The three phenomena mainly responsible for acoustic damping in high-frequency combustion instabilities are the nozzle losses, the thermo-viscous losses at walls, and the turbulence/acoustic interaction at the jets. A fourth phenomenon not addressed here is the absorption of acoustics by the injection plate and will be tackled in the future of this work. For a compact nozzle applicable to transverse waves, an impedance model has been pro-

posed and allows to find analytic and numerical predictions. The visco-thermal losses are also modeled and compared to the literature prediction but must be reinforced by accounting for the near-wall turbulence. Finally, a strategy is under development for the analysis of jet absorption. Moreover, it will be necessary to also evaluate the losses due to scattering and refraction of the dominant acoustic mode towards other frequencies. Applications and comparisons will be made later with LES in progress calculations.

The presented low order framework can be augmented by using conservation equations on the velocity's contributions (mean, turbulence, acoustic, and entropy). It allows having an estimate of the amount of vorticity and entropy produced at the level of the jets and flames, absorbing part of the acoustics, being convected by the mean flow through the combustion chamber, and interacting back with the acoustics when reaching the nozzle.

8. ACKNOWLEDGMENT

This work is part of an ongoing PhD thesis at EM2C laboratory, cofounded by CNES, the French National Space Agency and ArianeGroup. A part of this work was performed using HPC resources from the mesocentre computing center of Ecole CentraleSupélec and Ecole Normale Supérieure Paris-Saclay supported by CNRS and Région Ile-de-France.

9. REFERENCES

[1] L. Crocco and S.-I. Cheng. Theory of combustion instability in liquid propellant rocket motors. *Butterworths Scientific Publications*, 1956.

[2] D.T. Harrje and F.H. Reardon. Liquid Propellant Rocket Combustion Instability. *Technical Report SP-194, NASA*, 1972.

[3] J.C. Oefelein and V. Yang. Comprehensive review of liquid-propellant combustion instabilities in F-1 engines. *Journal of Propulsion and Power*, 9(5):657–677, 1993.

[4] Y. Méry. Mécanismes d'instabilités de combustion haute-fréquence et application aux moteurs-fusées. *Ph.D. thesis, Ecole Centrale Paris*, 2010.

[5] F.E.C. Culick. Unsteady Motions in Combustion Chambers for Propulsion Systems. *NATO Research and Technonoly Organization*, (AC/323 (AVT-039) TP/10), 2006.

[6] T. Poinsot and D. Veynante. Theoretical and Numerical Combustion. *Edwards*, 2nd edition, 2005.

[7] K. R. McManus, T. Poinsot, and S. M. Candel. A review of active control of combustion instabilities. *Progress in Energy and Combustion Science*, 19(1):1–29, 1993.

[8] B.-T. Chu and L.S.G. Kovasznay. Non-linear interactions in a viscous heat-conducting compressible gas. *Journal of Fluid Mechanics*, 3(5):494–514, 1958.

[9] F.E. Marble and S. Candel. Acoustic disturbance from gas non-uniformities convected through a nozzle. *Journal of Sound and Vibration*, 55(2):225–243, 1977.

[10] R. Nez, M. Gonzalez-Flesca, D. Marchal, T. Schmitt, P. Scouflaire, S. Candel, and S. Ducruix. Experimental and numerical characterizations of acoustic damping rates in a coupled-cavity configuration. *8th European Conference for Aeronautics and Aerospace Sciences (EUCASS)*, 2019.

[11] S.C.L. Webster. Analysis of pressure dynamics, forced excitation and damping in a high pressure LOx/H2 combustor. *Ph.D. Thesis, RWTHAACHEN University*, 2016.

[12] J. Li, D. Yang, C. Luzzato, and A.S. Morgans. Open Source Combustion Instability Low Order Simulator (OSCILOS-Long) Technical report Open Source Combustion Instability Low Order Simulator. *Imperial College, London, UK*, 2015.

[13] C. Laurent, M. Bauerheim, T. Poinsot, and F. Nicoud. A novel modal expansion method for low-order modeling of thermoacoustic instabilities in complex geometries. *Combustion and Flame*, 206:334–348, 2019.

[14] F. Nicoud, L. Benoit, C. Sensiau, and T. Poinsot. Acoustic Modes in Combustors with Complex Impedances and Multidimensional Active Flames. *AIAA Journal*, 45(2):426–441, 2007.

[15] B.T. Zinn and M.E. Lores. Application of the Galerkin Method in the Solution of Non-linear Axial Combustion Instability Problems in Liquid Rockets. *Combustion Science and Technology*, 4(1):269–278, 1971.

[16] L. Crocco and W.A. Sirignano. Behavior of supercritical nozzles under three-dimensional oscillatory conditions. *NATO AGARDograph*, 117, 1967.

[17] W.A. Bell and B.T. Zinn. The prediction of three-dimensional liquid-propellant rocket nozzle admittances. *NASA REPORT*, CR-121129, 1973.

[18] F. Nicoud and K. Wieczorek. About the zero Mach number assumption in the calculation of thermoacoustic instabilities. *International*

Journal of Spay and Combustion Dynamics, 1(1):67–112, 2009.

[19] I. Duran and S. Moreau. Solution of the quasi-one-dimensional linearized Euler equations using flow invariants and the Magnus expansion. *Journal of Fluid Mechanics*, 723:190–231, 2013.

[20] I. Duran and A.S. Morgans. On the reflection and transmission of circumferential waves through nozzles. *Journal of Fluid Mechanics*, 773:137–153, 2015.

[21] T. Sattelmayer, R. Kathan, S. Köglmeier, R. Kaess, and A. Nicole. Validation of Transverse Instability Damping Computations for Rocket Engines. *Journal of Propulsion and Power*, 31(4):1148–1158, 2015.

[22] S.R. Stow, A.P. Dowling, and T.P. Hynes. Reflection of circumferential modes in a choked nozzle. *Journal of Fluid Mechanics*, 467:215–239, 2002.

[23] G. Ghirardo, F. Boudy, and M. R. Bothien. Amplitude statistics prediction in thermoacoustics. *Journal of Fluid Mechanics*, 844:216–246, 2018.

[24] G. Bonciolini, A. Faure-Beaulieu, C. Bourquard, and N. Noiray. Low order modelling of thermoacoustic instabilities and intermittency: Flame response delay and nonlinearity. *Combustion and Flame*, 226:396–411, 2021.

[25] M. Schulze and T. Sattelmayer. Linear stability assessment of a cryogenic rocket engine. *International Journal of Spray and Combustion Dynamics*, 9(4):277–298, 2017.

[26] G. Kirchhoff. Ueber den Einfluss der Wämeleitung in Einem Gase ouf die Schallbewegung. *Annalen der Physik und Chemie*, (210):177–193, 1868.

[27] G. Searby, A. Nicole, M. Habiballah, and E. Laroche. Prediction of the efficiency of acoustic damping cavities. *Journal of Propulsion and Power*, 24(3):516–523, 2008.

[28] M.S. Howe. The damping of sound by wall turbulent shear layer. *The Journal of the Acoustical Society of America*, 98:1723–1730, 1995.

[29] F. Mbailassem, E. Gourdon, Q. Leclère, E. Redon, and T. Cambonie. Sound absorption prediction of linear damped acoustic resonators using a lightweight hybrid model. *Applied Acoustics*, 150:14–26, 2019.

[30] W.C. Reynolds and A.K.M.F. Hussain. The mechanics of an organized wave in turbulent shear flow. Part 3. Theoretical models and comparisons with experiments. *Journal of Fluid Mechanics*, 54(2):263–288, 1972.

[31] M.S. Howe. On the Absorption of Sound by Turbulence and Other Hydrodynamic Flows. *IMA Journal of Applied Mathematics*, 32(1-3):187–209, 1984.

[32] M.J. Lighthill. On the energy scattered from the interaction of turbulence with sound or shock waves. *Mathematical Proceedings of the Cambridge Philosophical Society*, 49(3):531–551, 1953.

[33] D.T. Noir and A.R. George. Absorption of sound by homogeneous turbulence. *Journal of Fluid Mechanics*, 86(3):593–608, 1978.

[34] C. Weng, S. Boij, and A. Hanifi. Application of the Galerkin Method in the Solution of Nonlinear Axial Combustion Instability Problems in Liquid Rockets. *The Journal of the Acoustical Society of America*, 4:269–278, 2013.

[35] S.C. Crow. Visco-Elastic Character of Fine-Grained Isotropic Turbulence. *Physics of Fluids*, 10(7), 1967.

[36] R.H. Kraichnan. Diffusion by a Random Velocity Field. *The Physics of Fluids*, 13(1):22–31, 1970.

[37] A. Smirnov, S. Shi, and I. Celik. Random Flow Generation Technique for Large Eddy Simulations and Particle-Dynamics Modeling. *Journal of Fluid Engineering*, 123(2):359–371, 2001.